

Spin-orbit effects in a graphene bipolar pn junction

A. YAMAKAGE¹, K.-I. IMURA^{1,2}, J. CAYSSOL² AND Y. KURAMOTO¹

¹ *Department of Physics, Tohoku University, Sendai, 980-8578, Japan*

² *Condensed Matter Theory Group, CPMOH, UMR 5798, Université Bordeaux I, 33405 Talence, France*

PACS 73.23-b – Electronic transport in mesoscopic systems

PACS 76.63.-b – Electronic transport in nanoscale materials and structures

PACS 73.40.-c – Electronic transport in interface structures

Abstract. – A graphene *pn* junction is studied theoretically in the presence of both intrinsic and Rashba spin-orbit couplings. We show that a crossover from perfect reflection to perfect transmission is achieved at normal incidence by tuning the perpendicular electric field. By further studying angular dependent transmission, we demonstrate that perfect reflection at normal incidence can be clearly distinguished from trivial band gap effects. We also investigate how spin-orbit effects modify the conductance and the Fano factor associated with a potential step in both *nn* and *np* cases.

Introduction. – There has been recent interest in a novel class of band insulators, called topological insulators (TIs) [1]. TIs are characterized by a bulk gap and a pair of time-reversed edge states at the boundary. These gapless edge states originate from the lattice spin-orbit (SO) effect and are protected by time-reversal symmetry from moderate disorder and interaction. In their seminal paper [2], Kane and Mele demonstrated that a graphene monolayer may become a TI when the intrinsic SO coupling dominates over the extrinsic Rashba coupling. Then the graphene layer is characterized by a Z_2 topological number [3] and has gapless edge states that disappear if the Rashba coupling becomes too large, or if Coulomb interactions exceed a certain threshold [4]. Therefore the existence of the topological phase in graphene depends crucially on the values of the intrinsic and extrinsic (Rashba) SO couplings. In the concluding section, we shall discuss recent estimates of these SO interactions which allows for considering the transition between the topological ($\Delta \geq \lambda_R$) and ordinary ($\lambda_R \geq \Delta$) phases.

Since the insulating regime is rather difficult to access experimentally, we propose to characterize this crossover by transport properties in the doped regime. In particular we stress that transport through a bipolar *pn* junction should differ in the distinct cases $\Delta \geq \lambda_R$ and $\lambda_R \geq \Delta$ respectively. Quasi-relativistic Klein tunneling [5] was demonstrated experimentally [6–12] by using local gating techniques, and the corresponding theory have received a great deal of attention [13–16] in the absence of SO cou-

pling ($\Delta = \lambda_R = 0$).

In this Letter, we obtain the angular dependent transmission of a *pn* junction in the presence of both intrinsic and Rashba SO couplings. At normal incidence, we show that the *pn* junction transmission exhibits a crossover from perfect reflection to perfect transmission when the Rashba coupling is tuned by the perpendicular electric field. We also predict the conductance and the Fano factor associated with a potential step in presence of intrinsic and Rashba SO couplings.

Similar topological phases have also been predicted [17] and now observed [18] in materials with larger SO interactions such as HgTe/CdTe quantum wells. The protected edge states appear when the width of the HgTe layer exceeds a critical value. We choose to study graphene since the Kane-Mele is the simplest possible model that have four spin-split bands, which is the minimum required for the nontrivial phase to exist [19,20]. Moreover our predictions might be compared to the studies of Klein tunneling in graphene performed in the absence of SO coupling ($\Delta = \lambda_R = 0$).

Kane-Mele model and single valley approximation. – The Kane-Mele model describes the low-energy dynamics of quasiparticles near the K and K' points of graphene in the presence of spin-orbit effects [2]. The corresponding Hamiltonian $H_{KM} = H_0 + H_{SO} + H_R$ acts on the slowly varying envelop $\psi(x, y)$ of electronic Bloch wavefunctions, which are indexed by real spin (Pauli matrices s_i , $i = x, y, z$), lattice isospin (σ_i) and valley isospin

(τ_i) quantum numbers. The kinetic Hamiltonian

$$H_0 = -i\hbar v_F \psi^\dagger (\sigma_x \tau_z \partial_x + \sigma_y \partial_y) \psi \quad (1)$$

describes massless Dirac fermions and is spin-independent. In the following we shall use units with $\hbar = v_F = 1$.

The intrinsic spin-orbit effect is completely determined by the symmetries of the honeycomb lattice and by the geometry of the carbon orbitals. It can be described by the Hamiltonian

$$H_{SO} = -\Delta \psi^\dagger \sigma_z \tau_z s_z \psi, \quad (2)$$

where 2Δ is the value of the gap induced at K (and K'). This form can be deduced from group theoretical techniques [2] or as the low-energy limit of tight-binding models [21–23]. It was shown recently that Δ can be increased by inducing a curvature of the graphene layer [22].

In the presence of a perpendicular electric field (generated by the distant gate), there is an additional Rashba spin-orbit coupling [24]

$$H_R = \lambda_R \psi^\dagger (\sigma_y s_x - \sigma_x \tau_z s_y) \psi, \quad (3)$$

where λ_R is proportional to the electric field.

In the following we shall restrict ourselves to transport through potential barriers which are smooth on the scale of the atomic lattice period. Therefore we shall neglect intervalley scattering by using a single-valley version of the Kane-Mele Hamiltonian H_{KM} wherein the eigenvalue of τ_z is replaced by $+1$ (or -1) for K (or K'). The resulting Hamiltonian $H_{KM}^{(K)}$ consists in a 4×4 matrix applying to spinors of the form ${}^t [\psi_{A\uparrow}, \psi_{B\uparrow}, \psi_{A\downarrow}, \psi_{B\downarrow}]$, where t represents transpose. Here the arrow index (\uparrow, \downarrow) stands for real spin while the index (A, B) denotes the two inequivalent sites of the honeycomb lattice.

Band structure. – In the homogeneous case, the two-dimensional momentum $\mathbf{p} = (p_x, p_y)$ is a good quantum number. The single valley Kane-Mele Hamiltonian $H_{KM}^{(K)}$ is diagonalized by the eigenspinors $|\alpha\beta\rangle_{\mathbf{p}}$ as

$$H_{KM}^{(K)} |\alpha\beta\rangle_{\mathbf{p}} = E_{\alpha\beta}(\mathbf{p}) |\alpha\beta\rangle_{\mathbf{p}}, \quad (4)$$

where $\alpha, \beta = \pm 1$ are band indices. The four energy bands are characterized by the dispersion

$$E_{\alpha\beta}(\mathbf{p}) = \alpha \sqrt{\mathbf{p}^2 + (\Delta + \beta \lambda_R)^2} + \beta \lambda_R, \quad (5)$$

where $\mathbf{p}^2 = p_x^2 + p_y^2$. The energy spectra has distinct features depending on the value of the ratio λ_R/Δ (Fig. 1).

In the absence of Rashba coupling, the intrinsic spin-orbit coupling opens a gap at $\mathbf{p} = \mathbf{0}$ separating the conduction band $E_{+\beta}(\mathbf{p}) = \sqrt{\mathbf{p}^2 + \Delta^2}$ from the valence band $E_{-\beta}(\mathbf{p}) = -\sqrt{\mathbf{p}^2 + \Delta^2}$, each one still having a two-fold degeneracy with respect to $\beta = \pm 1$.

A finite Rashba interaction generates a splitting of those bands which may eventually close the gap. In that sense the intrinsic and Rashba SO effects compete each other.

When the intrinsic SO dominates ($\Delta > \lambda_R$), the system is a band insulator whereas it is a gapless semimetal with quadratically dispersing bands in the opposite case ($\Delta < \lambda_R$). The intermediate case $\Delta = \lambda_R$ is rather special since two linearly dispersing bands $E_{\alpha-}(\mathbf{p}) = \alpha |\mathbf{p}| - \lambda_R$ are recovered. Nevertheless the system differs from the graphene spectrum in the absence of SO coupling $E(\mathbf{p}) = \pm v_F |\mathbf{p}|$ by the presence of two additional spin-split parabolic bands $E_{\alpha+}(\mathbf{p})$.

In coordinate representation, the eigenspinors $|\alpha\beta\rangle_{\mathbf{p}}$ are plane waves $\langle \mathbf{r} | \alpha\beta \rangle_{\mathbf{p}} = \Phi_{\beta}(E, \mathbf{p}) e^{i\mathbf{p}\cdot\mathbf{r}}$ with

$$\Phi_{\beta}(E, \mathbf{p}) = A(E, \mathbf{p}) \begin{bmatrix} p_x - ip_y \\ E + \Delta \\ -i\beta(E + \Delta) \\ -i\beta(p_x + ip_y) \end{bmatrix}, \quad (6)$$

and $\mathbf{p}\cdot\mathbf{r} = p_x x + p_y y$. The normalization factor is simply

$$A(E, \mathbf{p}) = \frac{1/\sqrt{2}}{\sqrt{|p_x|^2 + p_y^2 + (E(\mathbf{p}) + \Delta)^2}}.$$

Note that for a given energy E , the band index α is automatically determined. The spinor Eq. (6) also describes evanescent modes characterized by a purely imaginary p_x (superposed in broken curves in Fig. 1). Naturally, those modes cannot exist in an infinite sheet, but they develop in the presence of an interface (see below the interface between the $n-$ and $p-$ doped regions) and contribute to the scattering properties.

Eigenstates with different momentum or energy are obviously orthogonal to each other ${}_{\mathbf{p}}\langle \alpha\beta | \alpha'\beta' \rangle_{\mathbf{p}'} = \delta_{\alpha\alpha'} \delta_{\beta\beta'} \delta_{\mathbf{p}\mathbf{p}'}$. Here we emphasize that the eigenstates Eq. (6) of the Kane-Mele model satisfy an additional orthogonality relation: $\Phi_{\beta}^{\dagger} \Phi_{\beta'} = \delta_{\beta\beta'}$ when $p_y = 0$. Moreover the band indices α and β play very different roles: index β determines the symmetry of wave function, while α specifies whether the state belongs to the conduction or the valence band. In Fig. 1 (b), two energy bands with the same band index $\beta = -$ combine to form a linear Dirac spectrum. The orthogonality between eigenstates with different β also holds true for evanescent modes realized in the vicinity of pn -junction.

The pn -junction Model. – We now introduce our model of a pn -junction in a monolayer of graphene described within the Kane-Mele model. We assume that an electrostatic gate creates a potential barrier $V(x)$ which is smooth on the scale of the atomic lattice. Moreover we consider an ideally pure system, a situation which have been approached experimentally in suspended devices [25, 26]. Then no inter-valley scattering is involved, i.e. K and K' points are decoupled. One can use safely the single-valley approximation and describe the junction by the 4-band Hamiltonian

$$H(x) = H_{KM}^{(K)} + V(x) \psi^\dagger \psi, \quad (7)$$

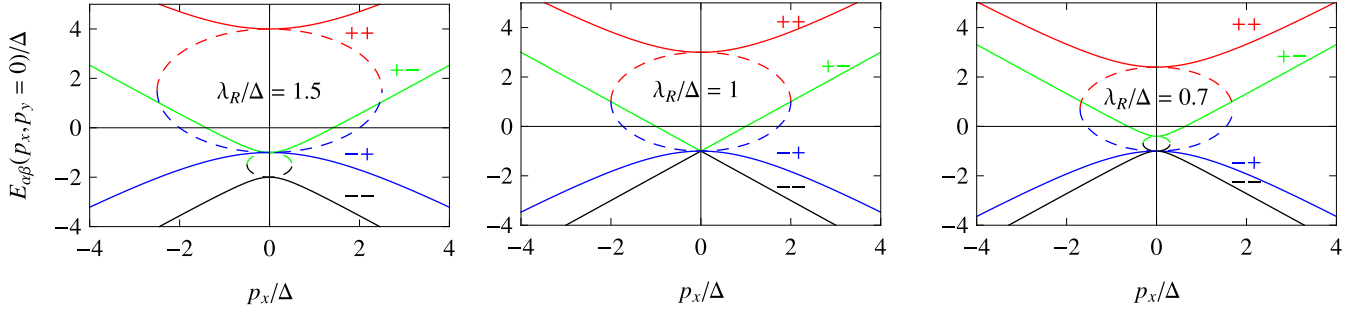


Fig. 1: Energy spectra for different values of $\lambda_R/\Delta = 1.5, 1, 0.7$. Propagating modes are shown in solid curves while evanescent modes are superposed in broken curves with p_x replaced by κ in Eq. (11). When Rashba coupling dominates the intrinsic SO interaction Δ (left panel), the spectrum is gapless and quadratic, whereas it is gapped in the opposite case (right panel). In the balanced case $\lambda_R = \Delta$ (central panel) the spectrum is gapless and hosts a Dirac cone.

where the $V(x)$ term is diagonal in both spin and lattice isospin degrees of freedom. Moreover we assume that the barrier is sharp on the scale of the Fermi wavelength in each of the metallic bands at right and left. In this sense, we shall investigate the scattering by an abrupt barrier defined by

$$V(x) = \begin{cases} 0 & (x < 0) \\ V_0 > 0 & (x > 0) \end{cases}. \quad (8)$$

Note that we also assume a straight interface with translational invariance along the y direction (no roughness along the interface $x = 0$).

Scattering states. – We investigate how incident fermions from the left are scattered by the potential barrier $V(x)$. The left side ($x < 0$) being always in the doped metallic regime, transport across the junction is dominated by extended two-dimensional waves while helical edge states are irrelevant here. Owing to translational invariance along the y axis, the momentum p_y is a good quantum number and factors $e^{ip_y y}$ can be omitted accordingly. We now construct scattering states at the Fermi level defined by their energy E and momentum p_y . We choose the energy E such that incident particles are injected from the single band $E_{+-}(\mathbf{p})$, which is realized for $-\Delta < E < 2\lambda_R + \Delta$.

The scattering state on the incident side takes the following form:

$$\Psi(x < 0) = \Phi^{(i)} e^{ikx} + r\Phi^{(r)} e^{-ikx} + r_{ev}\Phi^{(ev)} e^{\kappa x}, \quad (9)$$

where $\Phi^{(i)} = \Phi_-(E, \mathbf{p}_i)$, $\Phi^{(r)} = \Phi_-(E, \mathbf{p}_r)$, and $\Phi^{(ev)} = \Phi_+(E, \mathbf{p}_{ev})$. The wavevectors of the incident, reflected and evanescent waves are respectively $\mathbf{p}_i = (k, p_y)$, $\mathbf{p}_r = (-k, p_y)$ and $\mathbf{p}_{ev} = (-i\kappa, p_y)$, with

$$k = \sqrt{(E + \Delta)(E - \Delta + 2\lambda_R) - p_y^2}, \quad (10)$$

$$\kappa = \sqrt{p_y^2 - (E + \Delta)(E - \Delta - 2\lambda_R)}. \quad (11)$$

On the transmitted side, the wavefunction reads

$$\Psi(x > 0) = t_+\Phi^{(+)} e^{ip_+ x} + t_-\Phi^{(-)} e^{ip_- x}, \quad (12)$$

where $\Phi^{(\beta)} = \Phi_\beta(E - V_0, \mathbf{p}_\beta)$ and $\mathbf{p}_\beta = (p_{x\beta}, p_y)$ are amplitude and wavevector of the two transmitted waves $\beta = \pm$. The spinors $\Phi^{(+)}$ and $\Phi^{(-)}$ represent either a propagating or an evanescent (p_\pm becomes pure imaginary) mode depending on the sign of

$$p_{x\beta}^2 = (E - V_0 + \Delta)(E - V_0 - \Delta - 2\beta\lambda_R) - p_y^2. \quad (13)$$

If $p_{x\beta}^2 > 0$, the mode in the corresponding $E_{-\beta}(\mathbf{p})$ band is propagating. The actual sign of $p_{x\beta}$ is chosen such that the group velocity is positive, thereby describing an outgoing transmitted wave packet. In the specific case of inter-band tunneling, the positive group velocity is realized by a negative momentum state ($\alpha < 0$ in Eq. (5)) implying $p_{x\beta} < 0$. If $p_{x\beta}^2 < 0$, the mode in the corresponding $E_{-\beta}(\mathbf{p})$ band is evanescent.

Demanding continuity of the wavefunctions $\Psi(0^+) = \Psi(0^-)$ at the interface:

$$\Phi^{(i)} + r\Phi^{(r)} + r_{ev}\Phi^{(ev)} = t_+\Phi^{(+)} + t_-\Phi^{(-)}, \quad (14)$$

we obtain four independent scalar equations for the scattering parameters: r , r_{ev} , t_+ and t_- . Thus the reflection probability $R = |r|^2$ is determined uniquely from Eq. (14) for given E , V_0 and p_y .

Transmission at normal incidence. – We examine here the normal incidence transmission ($p_y = 0$) through the pn junction in the presence of Rashba and intrinsic SO effects. The pn junction is defined by Eq. (8) together with the condition $V_0 - E > \Delta$ to insure inter-band tunneling.

Decoupling at normal incidence. When $p_y = 0$, the continuity equation Eq. (14) reduces to two decoupled equations

$$r_{ev}\Phi^{(ev)} = t_+\Phi^{(+)}, \quad (15)$$

$$\Phi^{(i)} + r\Phi^{(r)} = t_-\Phi^{(-)}, \quad (16)$$

due to the symmetry of the spinors. Indeed, the full Hilbert space is the direct sum $\Omega = \Omega_+ \oplus \Omega_-$ of two orthogonal subspaces. The spinors $\Phi^{(ev)}$ and $\Phi^{(+)}$ belong to the subspace Ω_+ spanned by ${}^t[1, 0, 0, -i]$ and ${}^t[0, 1, -i, 0]$,

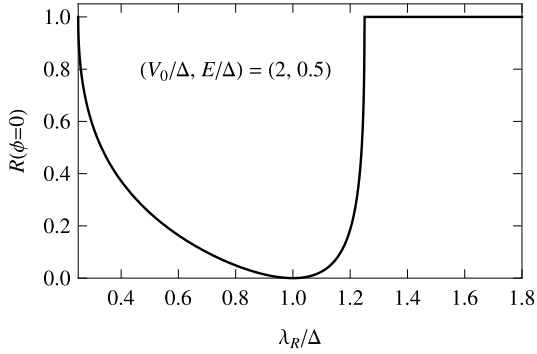


Fig. 2: Reflection probability $R(\phi = 0)$ of the pn junction as a function of λ_R/Δ , at normal incidence.

where t represents transpose. The spinors $\Phi^{(i)}$, $\Phi^{(r)}$ and $\Phi^{(-)}$ belong to the orthogonal subspace Ω_- spanned by $t[1, 0, 0, i]$ and $t[0, 1, i, 0]$.

Therefore solving Eq.(16) yields the following simple expression for the reflection amplitude at normal incidence

$$r = \frac{k(E - V_0 + \Delta) - p_{x-}(E + \Delta)}{k(E - V_0 + \Delta) + p_{x-}(E + \Delta)}, \quad (17)$$

where k and p_{x-} are obtained by substituting $p_y = 0$ in Eqs.(10,13).

Dominant Rashba effect. At large enough Rashba coupling, namely $\lambda_R > (\Delta + V_0 - E)/2$, there is one propagating ($\Phi^{(+)}$) and one evanescent ($\Phi^{(-)}$) transmitted waves, momenta p_{x+} and p_{x-} being respectively real and purely imaginary. As a result, Eq.(17) yields unimodular reflection amplitude r , thereby indicating perfect reflection. This nontrivial total reflection arises because the only propagating transmitted wave ($\Phi^{(+)}$) is orthogonal to the incident wave ($\Phi^{(i)}$) at normal incidence. This situation is similar to inter-band tunneling in bilayer graphene as we shall discuss later. For smaller Rashba coupling $\Delta < \lambda_R < (\Delta + V_0 - E)/2$, both transmitted waves are propagating leading to finite transmission through the $\Phi^{(-)}$ wave. Accordingly the momentum p_{x-} is real and Eq.(17) implies partial reflection, i.e. $0 < |r|^2 < 1$.

Balanced Rashba and intrinsic SO effects. At $\lambda_R = \Delta$, the bands $E_{\alpha-}$ become linear $E_{\alpha-}(\mathbf{p}) = \alpha|\mathbf{p}| - \Delta$ and combine to form a Dirac cone. Meanwhile, the spinors show further orthogonality relations in addition to the one with respect to β . Namely, at this particular value the reflected wave becomes orthogonal to the incident wave, thereby implying perfect transmission. In the case of (mono-layer) graphene in the absence of SO effects, the total absence of backscattering at normal incidence is due to the chiral symmetry, i.e. $T^2 = -1$ (T : time-reversal operator), and Berry phase π [13, 27]. Another important consequence of chiral symmetry is the anti-localization in the absence of inter-valley scattering [29]. Here, in the Kane-Mele model, $T^2 = 1$ and the Berry phase is 2π , due to the activation [30] of real spin by Rashba SO coupling.

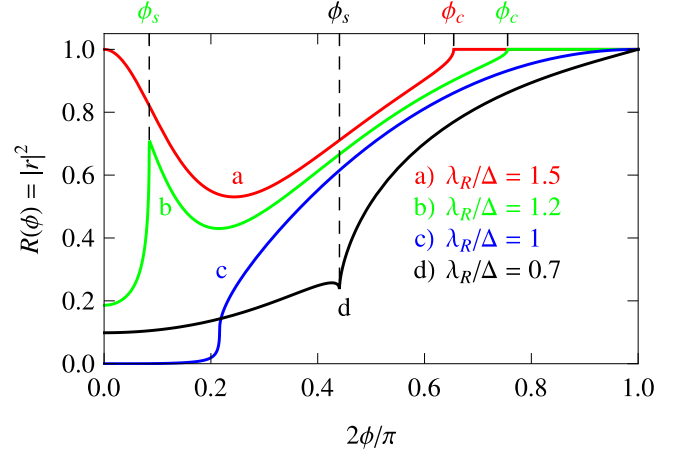


Fig. 3: Angular dependence of the reflection probability $R(\phi) = |r|^2$. $R(\phi)$ is plotted at $(V_0/\Delta, E_0/\Delta) = (2, 0.5)$ for different values of $\lambda_R/\Delta = 1.5, 1.2, 1, 0.7$. Four different types of behaviors can be seen: (a) crossover from perfect reflection to partial transmission with a broad dip ($\lambda_R/\Delta = 1.5$), (b) a peak in $R(\phi)$ ($\lambda_R/\Delta = 1.2$), (c) crossover from perfect to partial transmission ($\lambda_R/\Delta = 1$), and (d) a cusp like dip in $R(\phi)$ ($\lambda_R/\Delta = 0.7$).

As a result the system shows standard weak localization in the absence of inter-valley scattering [30].

Topological gap phase. At large intrinsic SO coupling $\lambda_R < \Delta$, both $\Phi^{(+)}$ and $\Phi^{(-)}$ describe propagating waves. Therefore the reflection is only partial.

Summarizing this section, we have seen that the pn junction shows a crossover from perfect reflection at large Rashba coupling towards perfect transmission when $\lambda_R = \Delta$, while finite reflection is restored at smaller values of the Rashba coupling (Fig. 2). These contrasted behaviors are reminiscent of those of a pn junction in single and bilayer graphene which show respectively perfect transmission and perfect reflection at normal incidence [13, 28]. These remarkable features originate from the orthogonality between the incident and scattered spinors at normal incidence. However, this orthogonality relation between $\Phi_+(E, \mathbf{p})$ and $\Phi_-(E, \mathbf{p})$ is broken as soon as p_y becomes finite.

It is worthy to note that the parameter $i\lambda_R$ in the Kane-Mele model plays formally the role of inter-layer hopping in bilayer graphene. Thus monolayer graphene with only Rashba SO has the same structure as that of spinless bilayer graphene, and shows the same charge transport properties.

Transmission at arbitrary incidence. – We now focus on the angular dependence of the transmission through a bipolar pn junction. The reflection probability $R(\phi) = |r|^2$ is obtained by solving the continuity equation Eq.(14), the incident angle ϕ satisfying $p_y = k \sin \phi$.

Dominant Rashba effect ($\lambda_R > \Delta$). As discussed previously the pn junction exhibits a perfect reflection

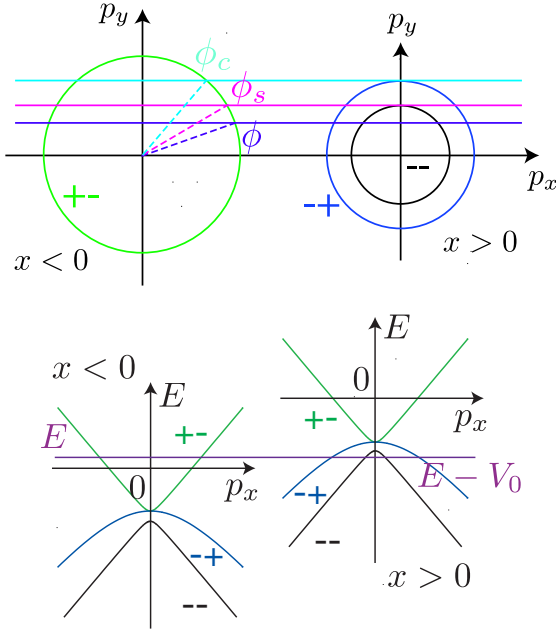


Fig. 4: Fermi circles (upper panel) and energy bands (lower panel) for intermediate Rashba coupling: $\Delta < \lambda_R < (\Delta + V_0 - E)/2$ on both sides of the junction. When incident angle ϕ is smaller than a critical value ϕ_s , both of the transmitted states are propagating. At $\phi = \phi_s$, $\Phi^{(-)}$ mode turns to evanescent. When ϕ exceeds ϕ_c , both of the transmitted states become evanescent. A pair of + or - indices refer to the band indices $\alpha\beta$.

at normal incidence for large enough Rashba coupling $\lambda_R > (\Delta + V_0 - E)/2$. As one varies the incident angle ϕ from normal incidence ($\phi = 0$), the reflection coefficient decreases and the curve $R(\phi)$ exhibits a broad dip (curve $\lambda_R/\Delta = 1.5$, Fig. 3.a). This feature clearly distinguishes the perfect reflection due to orthogonality in the normal incidence from the perfect reflection due to a band gap on the transmitted side. In the case of perfect reflection due to band gap, the reflection probability remains trivially equal to unity when one varies the incident angle ϕ away from normal incidence. At large incidence $\phi > \phi_c$, one recovers total reflection. The critical angle ϕ_c is determined by a condition on the Fermi wavevectors in the bands E_{+-} and E_{-+} as shown in Fig. 4.

For intermediate Rashba coupling $\Delta < \lambda_R < (\Delta + V_0 - E)/2$, reflection is only partial at $\phi = 0$ and the curve $R(\phi)$ exhibits a peak (curve $\lambda_R/\Delta = 1.2$, Fig. 3.b). The initial increase of $R(\phi)$ from $\phi = 0$ to ϕ_s is related to the overlap between the incident wave and transmitted ($\Phi^{(+)}$ and $\Phi^{(-)}$) waves. At small incidence, the dominant effect is the reduction of the overlap with the $\Phi^{(-)}$ mode yielding an increasing reflection probability. The local maximum of $R(\phi)$ at $\phi = \phi_s$ appears when the $\Phi^{(-)}$ mode turns to evanescent (Fig. 4, upper panel). For slightly larger incidence $\phi > \phi_s$, the dominant effect is the increase of the overlap between the incident wave and the (propagating)

transmitted $\Phi^{(+)}$ mode, thereby providing a decrease of $R(\phi)$. Above the critical angle $\phi > \phi_c$, both transmitted modes become evanescent at $x > 0$, thereby leading to $R(\phi) = 1$ (Fig. 4).

Balanced case ($\lambda_R = \Delta$). When $\lambda_R = \Delta$, the property of perfect transmission (which is exact at $\phi = 0$) pertains quite accurately to a broad range around normal incidence (curve $\lambda_R/\Delta = 1$, Fig. 3.c).

Topological gap phase ($\lambda_R < \Delta$). When $\lambda_R < \Delta$, the reflection probability $R(\phi)$ shows a sharp dip (curve $\lambda_R/\Delta = 1.2$, Fig. 3.d) at the angle ϕ_s where Φ^{-} mode turns to evanescent (Fig. 4, upper panel). The nature of this singularity is similar to that of peak structure at intermediate Rashba coupling already discussed. The singularity appears when $E - (\Delta - 2\lambda_R) > -\Delta - (E - V_0)$, which means $\lambda_R/\Delta > 0.5$ for $(V_0/\Delta, E_0/\Delta) = (0.5, 2)$. Note that E_{+-} and E_{--} bands are symmetric w.r.t. $E = -\lambda_R$.

Conductance and shot noise. – The conductance $G(V_0)$ and the Fano factor $F(V_0)$ associated with the potential step are readily obtained from the transmission probability, as described in [13–16]. In the balanced case $\lambda_R = \Delta$, the conductance curves $G(V_0)$ (Fig. 5, left panel) do not differ significantly from the case of no SO effects ($\lambda_R = \Delta = 0$) [15, 16]. In contrast, the vanishing of the conductance within a finite range of V_0 reveals that graphene is gapped when intrinsic SO dominates Rashba coupling. The Fano factor is, on the other hand, not well-defined in the gap. The Rashba dominated regime also exhibits anomalous features: a cusp in $G(V_0)$ and an enhancement of the Fano factor. The peak in $F(V_0)$ is rather asymmetric with a characteristic shoulder that broadens when increasing the Rashba coupling (Fig. 5, $\lambda_R/\Delta = 1.2, 1.5$).

The corresponding experiments should be done on graphene with very low absolute Fermi energies on both sides of the junction. Therefore disorder may hinder the observation of the crossover from perfect reflection to perfect transmission at the pn -junction [32]. Nevertheless ongoing progress in sample preparation might eventually render the spin-orbit effects observable in suspended graphene devices [25, 26]. The SO interaction is commonly supposed to be weak owing to the low atomic number of carbon. Nevertheless, first estimates indicated the favorable conditions for the TI to exist, namely a sizeable spin-orbit gap $2\Delta \sim 1$ K at the K, K' points and a tiny Rashba splitting $\lambda_R \sim 0.5$ mK for a typical electric field $E = 50$ V/300 nm [2]. Unfortunately due to the specific geometry of s and p orbitals in graphene, the actual intrinsic SO coupling should be far smaller, namely $2\Delta \sim 10$ mK, while the Rashba splitting is enhanced to typical values $\lambda_R \sim 70$ mK for $E = 50$ V/300 nm [21–23]. Recently, first-principle calculations suggested that d orbitals might play a dominant role in the gap opening at K and K' points [31]. As a result, the spin couplings are predicted to assume intermediate values ($2\Delta \sim \lambda_R \sim 0.1$ K) between the estimates of [2] and of [21–23]. Such close values and the possibility

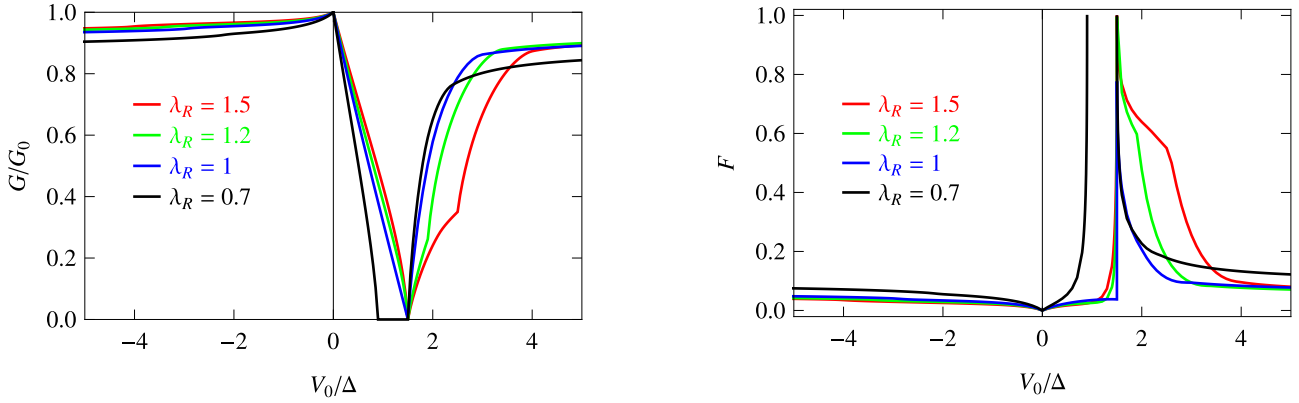


Fig. 5: Conductance G (left) and Fano factor F (right) of the junction for $E = 0.5\Delta$, and different values of $\lambda_R/\Delta = 1.5, 1.2, 1, 0.7$. The maximal conductance is given by $G_0 = (2e^2/\pi h)k_F W$ where W is the sample width (along y), and k_F is the Fermi wavevector in the left side ($x < 0$).

to tune both Rashba and intrinsic SO couplings allows to consider the transition between the topological ($\Delta \geq \lambda_R$) and ordinary ($\lambda_R \geq \Delta$) phases.

Concluding remarks. – We have shown that at normal incidence the pn junction transmission exhibits a crossover from perfect reflection at large Rashba coupling to perfect transmission when the Rashba coupling exactly balances the intrinsic spin orbit coupling. Further study on the angular dependence enabled us to clearly distinguish such unique features from trivial band gap effects. Finally we have obtained the conductance and the shot noise associated with an electrostatic potential step realized in a graphene monolayer with competing spin-orbit effects.

* * *

A.Yamakage and K.I. Imura are supported by KAKENHI (A.Yamakage: No. 08J56061 of MEXT, Japan, K.I. Imura: Grant-in-Aid for Young Scientists B-19740189). J. Cayssol acknowledges gratefully support from the Institut de Physique Fondamentale (IPF) in Bordeaux.

REFERENCES

- [1] M. König, H. Buhmann, L.W. Molenkamp, T.L. Hughes, C.X. Liu, X.L. Qi and S.C. Zhang, *J. Phys. Soc. Jpn* **77**, 031007 (2008).
- [2] C.L. Kane and E.J. Mele, *Phys. Rev. Lett.* **95**, 226801 (2005).
- [3] C.L. Kane and E.J. Mele, *Phys. Rev. Lett.* **95**, 146802 (2005).
- [4] C. Wu, B.A. Bernevig and S.-C. Zhang, *Phys. Rev. Lett.* **96**, 106401 (2006).
- [5] O. Klein, *Z. Phys.* **53**, 157 (1929).
- [6] B. Huard et al., *Phys. Rev. Lett.* **98**, 236803 (2007).
- [7] J.R. Williams, L. DiCarlo, and C.M. Marcus, *Science* **317**, 638 (2007).
- [8] B. Ozyilmaz et al., *Phys. Rev. Lett.* **99**, 166804 (2007).
- [9] J.B. Oostinga et al., *Nature Mat.* **7**, 151 (2008).
- [10] R. V. Gorbachev et al., *Nano Lett.* **8**, 1995 (2008).
- [11] N. Stander, B. Huard, and D. Goldhaber-Gordon, *Phys. Rev. Lett.* **102**, 026807 (2009).
- [12] G. Liu et al., *Appl. Phys. Lett.* **92**, 203103 (2008).
- [13] M.I. Katsnelson, K.S. Novoselov, and A.K. Geim, *Nature Phys.* **2**, 620 (2006).
- [14] V.V. Cheianov, V.I. Falko, *Phys. Rev. B* **74**, 041403(R) (2006).
- [15] J. Cayssol, B. Huard, and D. Goldhaber-Gordon, *Phys. Rev. B* **79**, 075428 (2009).
- [16] E.B. Sonin, *Phys. Rev. B* **79**, 195438 (2009).
- [17] B. A. Bernevig, T. L. Hughes, and S.C. Zhang. *Science* **314**, 1757 (2006).
- [18] M. König, S. Wiedmann, C. Brüne, A. Roth, H. Buhmann, L. Molenkamp, X.-L. Qi, and S.C. Zhang, *Science* **318**, 766 (2007).
- [19] S. Murakami et al., *PRB* **76**, 205304 (2007).
- [20] X.-L. Qi et al., *PRB* **78**, 195424 (2008).
- [21] H. Min, J.E. Hill, N.A. Sinitsyn, B.R. Sahu, L. Kleinman, and A.H. MacDonald, *Phys. Rev. B* **74**, 165310 (2006).
- [22] D. Huertas-Hernando, F. Guinea, and A. Brataas, *Phys. Rev. B* **74**, 155426 (2006).
- [23] Y. Yao, F. Yei, X.L. Qi, S.C. Zhang, and Z. Fang, *Phys. Rev. B* **75**, 041401(R) (2007).
- [24] Y.A. Bychkov and E.I. Rashba, *JETP. Lett.* **39**, **78** (1984).
- [25] X. Du et al., *Nature Nanotechnology* **3**, 491 - 495 (2008).
- [26] K. I. Bolotin et al., *Phys. Rev. Lett.* **101**, 096802 (2008).
- [27] T. Ando, T. Nakanishi and R. Saito, *JPSJ* **67**, 2857 (1998).
- [28] A. H. Castro Neto, F. Guinea, N. M. Peres, K. S. Novoselov, and A. K. Geim, *Rev. Mod. Phys.* **81**, 109 (2009).
- [29] H. Suzuura, T. Ando, *Phys. Rev. Lett.* **89**, 266603 (2002).
- [30] K. I. Imura, Y. Kuramoto and K. Nomura, *Phys. Rev. B* **80**, 085119 (2009)
- [31] M. Gmitra, S. Konschuh, C. Ertler, C. Ambrosch-Draxl, and J. Fabian, arXiv:0904.3315.
- [32] J. Martin et al., *Nature Physics* **4**, 144 - 148 (2008).